

Dark state in ruby: Analysis of the feasibility

R. N. Shakhmuratov,^{1,2} A. Szabo,³ G. Kozyreff,⁴ R. Coussement,¹ J. Odeurs,¹ and Paul Mandel⁴

¹*Instituut voor Kern- en Stralingsfysica, Katholieke Universiteit Leuven, Celestijnenlaan 200 D, B-3001 Leuven, Belgium*

²*Kazan Physical-Technical Institute, Russian Academy of Sciences, 10/7 Sibirsky Trakt Street, Kazan 420029, Russia*

³*Institute for Microstructural Sciences, National Research Council of Canada, Ottawa, Ontario, Canada K1A0R6*

⁴*Optique Nonlinéaire Théorique, Université Libre de Bruxelles, Campus Plaine Case Postale 231, B-1050 Bruxelles, Belgium*

(Received 10 March 2000; published 15 September 2000)

Bichromatic excitation of the R_1 line in ruby at liquid-helium temperature is considered. The frequency difference of the spectral components of the driving field is resonant with the energy gap between the anti-crossed spin sublevels $+1/2$ and $+3/2$ in the ground state 4A_2 . The condition of the spin coherence trapping in the nonabsorbing state is analyzed. Population trapping is revealed in the reduced spontaneous emission from the excited state and in large spin magnetization of the ground state Cr^{3+} precessing with the frequency difference of the spectral components of the driving field. This magnetization can be detected by a pickup coil. The lifetime of the induced magnetization is strongly dependent on the ratio of the lifetime of the excited state \bar{E} and the spin coherence decay time $(T_2)_{spin}$.

PACS number(s): 42.50.Md, 42.50.Gy, 32.80.Bx, 33.80.Be

I. INTRODUCTION

While the resonant excitation of the two-level system has been studied comprehensively, the dynamics and kinetics of the three-level excitation are not obvious and disclose some features that are hard to explain within the pseudospin vector model or by the Bloch-vector model [1]. One of these examples is population trapping that was observed in sodium vapor [2–4]. Bichromatic excitation with a frequency difference matching the hyperfine splitting of ground-state sodium is quenched due to the accumulation of all the atoms in a particular superposition of the ground sublevels [5,6]. This effect takes place if two key conditions are satisfied. First, the excitation to the upper state must start from the two different sublevels of the ground state, i.e., the splitting and consequent interference of the quantum transition paths are to be present. Second, the lifetime of the sublevels coherence is to be longer than the lifetime of the excited state. The former condition creates this coherence and provides its selective phase-sensitive excitation. The latter condition allows the population of the dark state by spontaneous emission from the excited state if it is fast enough to compete with the coherence decay rate. The dark state has a particular phase satisfying the condition of destructive interference for the transition paths starting from these sublevels. Therefore, this state does not interact with the driving field.

In this paper, we analyze the possibility of creating the dark state in solids with paramagnetic impurities. While the transition splitting (branching) is easy to find for many impurities, the condition on the lifetime of the excited state and the relaxation time of the ground-state sublevels coherence seems harder to satisfy. Many optical transitions of paramagnetic impurities have long-lived excited states and strong contributions to the coherence dephasing coming from the crystal phonons or spin-spin interactions with the nearest neighbors in the host crystal. The phonon contribution can be eliminated by cooling the sample down to liquid-helium temperature. The spin-spin interactions can be reduced by a strong microwave excitation [7–9]. Laser excitation is also

capable of reducing the coherence decay. For example, appreciable coherent optical pumping of the resonant transitions in $\text{Pr}^{3+}:\text{LaF}_3$ and ruby reduces the homogeneous dephasing to the limit of the natural broadening [10–12]. These effects are similar to the motional narrowing [13] and one can find their explanation, for example, in [14–23] (the list is not exhaustive). The crucial point of most of these theories is that the field-driven impurity undergoes a fast Rabi oscillation between resonant levels that averages out the hyperfine interaction of the impurity with neighbors responsible for the coherence dephasing.

Suppression of the dephasing was studied by free-induction decay, following a long pulse excitation [7–11], and by a pump-probe sequence with the probe measuring the width of the hole burnt by the pump pulse [12]. The hole width measured in both kinds of experiments was much narrower than that predicted by the optical Bloch equations (OBE). This anomaly in the saturation of the absorption line width is easy to explain by assuming that the coherence dephasing has decreased. In fact, according to the OBE, in the strong saturation limit ($\chi^2 T_1 T_2 \gg 1$, where χ is Rabi frequency, T_1 and T_2 are the relaxation times of the population difference and of the coherence, respectively) the half-width at half maximum (HWHM) of the hole is close to $\chi \sqrt{T_1/T_2}$ [1,10]. Since the ratio T_1/T_2 is usually large for solids, the HWHM of the hole must be much larger than the Rabi frequency. However, experiments show a much narrower hole with HWHM $\sim \chi$. As $1/T_2 = 1/(2T_1) + \Gamma_{env}$, where Γ_{env} is a contribution of the environment to the coherence dephasing and $\Gamma_{env} \gg 1/T_1$, one can assume that a strong excitation decouples the impurity from this environment and the value Γ_{env} tends to zero at high excitation.

In these experiments, the influence of the field noise [24,25] and the field enhancement of the dipole-dipole interaction with nonresonant ions [24,26] are present. Both effects also result in the anomalous free-induction decay and hole burning because they contribute equally to the $1/T_1$ and $1/T_2$ relaxation processes. If their contribution Γ_{driven} is dominant ($\Gamma_{driven} \gg 1/T_1, 1/T_2$), then the hole also narrows.

Consequently, the motional narrowing may turn out to be a questionable explanation of the experiments [7–12].

From this viewpoint, new experiments sensitive to the motional narrowing and not affected favorably by the field noise and enhanced dipole-dipole interaction are particularly interesting. In this context, the population trapping in the dark state is the best way to verify the motional narrowing hypothesis because the dark state is populated by spontaneous emission from the excited state and can be affected by the field noise and the enhanced dipole-dipole interaction only destructively in contrast to the free-induction decay and hole burning. The negative effect of the field noise and enhanced dipole-dipole interaction on the population trapping in the dark state is due to the fact that both processes contribute to the decay of the coherence related to the dark-state existence.

In Sec. II, we consider the excitation scheme of ruby appropriate for the population trapping. Section III presents the master equations for the selected scheme. Dynamical evolution of the chromium impurity under the bichromatic excitation is considered in Sec. IV. The evolution of the nonresonant impurities is studied in Sec. V. The calculation of the spin magnetization induced by the bichromatic pumping is presented in Sec. VI. The steady-state analysis providing the condition of population trapping in the stationary state is presented in Sec. VII. The kinetic stage of the spin coherence evolution is discussed in Sec. VIII.

II. SPIN COHERENCE EXCITATION IN RUBY BY OPTICAL PUMPING

We consider the R_1 line in ruby related to the optical transition from the ground state 4A_2 to the excited state $\bar{E}({}^2E)$. One can find the ruby spectrum and the state notations, for example, in Refs. [27,28]. The ground and excited states have effective spins of $3/2$ and $1/2$, respectively. If a magnetic field is applied parallel to the trigonal (optical) axis of the ruby crystal, the splittings of the 4A_2 , \bar{E} energy levels are linear functions of the field, as shown Fig. 1. We follow the Schulz-DuBois notation [28] that identifies the ground-state energy levels by quantum number \bar{m} ranging from $-3/2$ to $+3/2$ in order of increasing energy. The number \bar{m} coincides with the quantum number m of the Zeeman Hamiltonian in the high-field limit.

In the ground state, the level $\bar{m} = +3/2$ crosses the levels $\bar{m} = -1/2$ and $\bar{m} = +1/2$ at 2.07 and 4.14 kG, respectively. If the magnetic field makes a small angle θ with the optical axis, defined as the z axis for the chromium spins, these levels mix and repulse at the crossings, then avoiding their intersection, i.e., anticrossings take place. At the field corresponding to the smallest separation between the energy levels, the eigenvectors of the total Hamiltonian consist of equal amplitudes of the unperturbed eigenvectors defined far from the crossing with respect to the z axis. For example, at the second crossing one has

$$|1\rangle = \frac{1}{\sqrt{2}}(|+1/2\rangle_G - |+3/2\rangle_G), \quad (1)$$

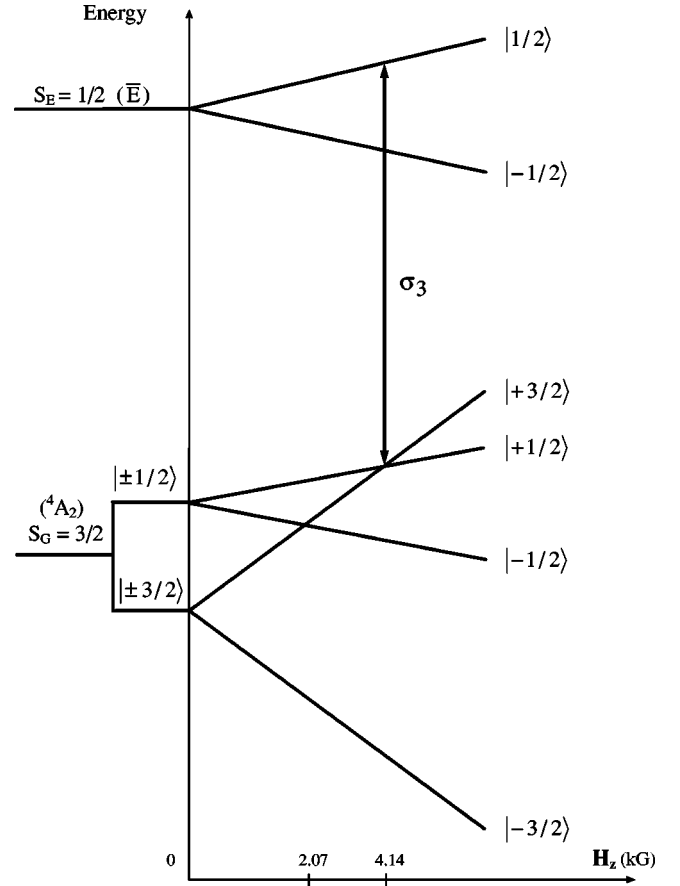


FIG. 1. Zeeman splitting of the 4A_2 and \bar{E} states of Cr^{3+} in ruby versus the magnetic field H , if \mathbf{H} is parallel to the optical axis. The zero-field splitting $2D$ of the ground-state spin sublevels is shown on the left of the plot. The transition between the 4A_2 and \bar{E} states for circularly σ^- (left) polarized light, propagating along the optical axis, is shown by the arrow.

$$|2\rangle = \frac{1}{\sqrt{2}}(|+1/2\rangle_G + |+3/2\rangle_G), \quad (2)$$

where $|+1/2\rangle_G, |+3/2\rangle_G$ relate to the spin sublevels $\bar{m} = +1/2$ and $\bar{m} = +3/2$ of the ground state 4A_2 , respectively.

The R_1 transition is electric-dipole, spin and parity forbidden in the presence of a center of symmetry. However, due to the crystalline field, this symmetry is broken and the transition becomes allowed [27]. In the ruby lattice, a Cr^{3+} impurity substitutes an Al^{3+} . The crystal symmetry of ruby is rhombohedral with the Cr impurity being surrounded almost octahedrally by six nearest O^{2-} ions producing a strong cubic field. In addition to the cubic field, a small trigonal field is present due to the distortion of the octahedron. The axis of the trigonal field is the optic axis of ruby. The hemihedral part of the trigonal field mixes the parity of the states, permitting optical transitions that would be forbidden if the ion were at the center of inversion symmetry. The matrix elements of the dipole transitions were calculated in [27] and experimentally tested in [29].

If the ruby sample is cooled to the temperature of liquid helium, a tunable laser is capable of exciting each component of the R_1 line selectively by choosing proper frequency and polarization of the light (see, for example, Refs. [30] and [11,12]). A circularly polarized laser excites the transitions ${}^4A_2(\bar{m} = \pm 3/2) \rightarrow {}^2E(\bar{m} = \pm 1/2)$ and ${}^4A_2(\bar{m} = \pm 1/2) \rightarrow {}^2E(\bar{m} = \pm 1/2)$ designated by $\sigma_1(+3/2 \rightarrow +1/2)$, $\sigma_2(-1/2 \rightarrow -1/2)$, $\sigma_3(+1/2 \rightarrow +1/2)$, and $\sigma_4(-3/2 \rightarrow -1/2)$, which is in the order of increasing energy at high magnetic field [30]. The selection rules in some of the indicated transitions are not apparently fulfilled in respect to \bar{m} . This is because the \bar{m} indicates only the main component of the level. The electric dipole transition matrix element is not zero due to the small admixture of the state with another parity and obviously with another \bar{m}' components. So, one can say that transition takes place due to the nonzero matrix elements between \bar{m} and \bar{m}' , where the latter is not shown explicitly in the wave-vector notation.

Far from anticrossings, we can excite the transition starting from only one spin sublevel of the ground state (for example, $|+1/2\rangle_G$) by choosing a proper frequency and polarization of the laser beam. At the anticrossing of this sublevel with another one, the induced transition splits into two paths involving both mixed states (for example, $|1\rangle$ and $|2\rangle$). Simultaneous excitation of two spin sublevels is capable of creating the spin states coherence. For example, a laser pulse may induce magnetization ringing at the level repulsion frequency, if the spectral width of the pulse is big enough to excite both transitions simultaneously.

Optically induced electron-spin magnetization was observed already, 35 years ago [31]. Ultrashort light pulses from a mode-locked ruby laser create a pulsed magnetization in a ruby sample at room temperature. This magnetization was measured by a pickup coil. Excitation by linearly polarized radiation [polarized parallel to the optical axis and exciting the transitions ${}^4A_2(\bar{m} = -1/2) \rightarrow {}^2E(\bar{m} = +1/2)$ and ${}^4A_2(\bar{m} = +1/2) \rightarrow {}^2E(\bar{m} = -1/2)$] revealed a sharp enhancement of the amplitude of the induced magnetization near the level anticrossings. Pumping by a circularly polarized beam along the optical axis near the anticrossings even allowed for resolving the oscillation of the induced precessing magnetization [32]. The precession frequency was in good agreement with the level repulsion energy. Near the second anticrossing, the time evolution of the $M_x(t)$, $M_y(t)$, and $M_z(t)$ components of the magnetization were examined separately by changing the direction of the pickup coil, where the x direction is defined by the transverse component of the magnetic field with respect to the optical axis (defined as the z direction). Similar signals for the $M_z(t)$ component were also observed in the vicinity of the first anticrossing point at 2.07 kG. Since the anticrossing levels in this case are $\bar{m} = +3/2$ and $\bar{m} = -1/2$, so $\Delta\bar{m} = 2$, detectable magnetization in the transverse xy plane can not be expected. This was actually the case.

In this paper, we show that cw optical excitation can also induce a precessing magnetization. Depending on the relax-

ation parameters of the system, this precession may be persistent, revealing the capture of the chromium impurities in the dark state.

We consider the second crossing to be able to detect all components of the induced magnetization. Below, we discuss the conditions of this excitation to choose the most effective scheme. At liquid-helium temperature, a linearly polarized laser beam (polarized parallel to the optical axis) may be tuned to induce preferentially the transition $+1/2({}^4A_2) \rightarrow -1/2(\bar{E})$. However, because the transition matrix elements are larger for the excitation by means of circularly polarized light, we choose the σ_3 transition [$+1/2({}^4A_2) \rightarrow +1/2(\bar{E})$], which can be also selectively excited by the left-hand polarized beam.

It was shown [33] for another system with hyperfine level (nuclear spin level) crossing that monochromatic excitation starting from the anticrossed states is capable of creating giant nuclear-spin polarization in the spin component that cannot be excited by laser light of the chosen polarization (dark state). The crossing of the $-1/2$ and $-3/2$ nuclear-spin levels were considered and excitation started from the $-3/2$ component.

In case of ruby, one may try to create a suitable condition for the population trapping in the dark state in a similar way. Choosing, for example, the excitation of the spin component $+1/2({}^4A_2)$ of the state vectors, Eqs. (1) and (2), by a σ^- -polarized laser beam, applied along the z axis, we expect that the resonant chromium impurities will be accumulated in the $+3/2({}^4A_2)$ component of the ground-state spin. The latter cannot be excited by the applied laser beam because of the selection rules. This component, the dark state, is the superposition of the mixed states

$$|+3/2\rangle_G = \frac{1}{\sqrt{2}}(|2\rangle - |1\rangle). \quad (3)$$

The fact that this dark state cannot be excited by the laser can be interpreted in terms of the destructive interference of the quantum paths $|1\rangle \rightarrow +1/2(\bar{E})$ and $|2\rangle \rightarrow +1/2(\bar{E})$. It is due to the coherence of the states $|1\rangle$ and $|2\rangle$. This particular coherence, Eq. (3), is created by a two-step process. First, the laser excitation starting from the spin component $|+1/2\rangle_G$ depopulates the coherent state

$$|+1/2\rangle_G = \frac{1}{\sqrt{2}}(|1\rangle + |2\rangle). \quad (4)$$

Second, spontaneous emission from the excited state $+1/2(\bar{E})$ can be terminated at any state, $|+1/2\rangle_G$ or $|+3/2\rangle_G$ because the direction and polarization of the emitted photon are not defined and may be anything. Interplay of both processes will lead eventually to the predominant population of the state $|+3/2\rangle_G$. This process is sensitive to the level repulsion frequency ω_{21} ($\hbar\omega_{21}$ is the energy interval between the levels $|2\rangle$ and $|1\rangle$) [33].

To explain this point, one has to consider the spin Hamiltonian of Cr^{3+} in the ground state 4A_2 . The spin-

Hamiltonian concept was introduced to describe electron-spin resonance spectra of the paramagnetic impurities [34]. As a result of ligand field interaction with the neighboring diamagnetic ions or atoms in a crystal, the ground state of a paramagnetic ion consists of a group of electronic levels whose separation is a few wave numbers or less, while all other electronic levels lie considerably higher. The behavior of this group can be represented by defining an effective spin S , such that the total number of levels in the group is $2S + 1$, the same as in an ordinary spin multiplet. It is further required that the matrix elements between the various states determined by the full Hamiltonian that describes the system shall be proportional to those of the effective spin. It is then possible to describe the behavior of this group of levels by a spin Hamiltonian involving just the effective spin. Therefore, the use of the symbol S for effective spin may be sometimes misleading. The ground-state spin Hamiltonian of Cr^{3+} [35] is

$$\mathcal{H} = g_z \beta H_z S_z + g_x \beta H_x S_x - D[S_z^2 - \frac{1}{3} S(S+1)], \quad (5)$$

where $S = 3/2$, $H_z = H \cos \theta$, and $H_x = H \sin \theta$ are longitudinal and transverse components of the magnetic field H , β is the Bohr magneton, $g_z = 1.984$, $g_x = 1.987$, $2D$ is a zero-field splitting ($D/h = 5.736$ GHz). The second term of the Hamiltonian, Eq. (5), is assumed to be small (since $\theta \ll 1$) and we consider it as a perturbation. As $\Delta \bar{m} = 1$ for the level crossing near 4.14 kG, the degeneracy of the crossed levels is removed in first order. The solution of the secular determinant yields the level repulsion energy

$$\hbar \omega_{21} = \sqrt{\bar{\Delta}^2 + \bar{V}^2}, \quad (6)$$

where $\bar{\Delta} = g_z \beta H_z - 2D$ and $\bar{V} = \sqrt{3} g_x \beta H_x$. The condition $\bar{\Delta} = 0$ corresponds to the closest approach of the levels when the splitting, Eq. (6), is determined only by the H_x component of the magnetic field and relevant eigenvectors are mixed according to Eqs. (1) and (2). Near the crossing, these eigenfunctions are

$$|1\rangle = \cos\left(\frac{\psi}{2}\right) |1/2\rangle_G - \sin\left(\frac{\psi}{2}\right) |3/2\rangle, \quad (7)$$

$$|2\rangle = \sin\left(\frac{\psi}{2}\right) |1/2\rangle_G + \cos\left(\frac{\psi}{2}\right) |3/2\rangle, \quad (8)$$

where $\tan \psi = \bar{V}/\bar{\Delta}$. According to the heuristic assumption expressed in [31], the additional change of magnetization M_z near the anticrossing is proportional to $a^2 b^2$, where $a = \cos \psi/2$ and $b = \sin \psi/2$ [the coefficients presented in expressions (7) and (8)]. In the next sections we show that even at equal population and excitation of the ground spin sublevels, the induced magnetization is large and proportional to the value $a^2 b^2$.

The second anticrossing can be described within a two-level approximation [32]. Using the model of a fictitious spin $\tilde{S} = 1/2$, the effective Hamiltonian can be written as

$$\mathcal{H}_{eff} = \tilde{g}_x \beta H_x \tilde{S}_x + g_z \beta \tilde{H}_z \tilde{S}_z, \quad (9)$$

where $\tilde{g}_x = \sqrt{3} g_x$ is an effective g factor for this spin, $\tilde{H}_z = H_z - 2(D/g_z \beta)$ is the effective longitudinal component of the magnetic field, and \tilde{S}_x and \tilde{S}_z are the x and z components of the fictitious spin. In these notations, the value ψ can be defined as the angle between the z axis and the effective field $\tilde{\mathbf{H}} = (H_x, 0, \tilde{H}_z)$.

If ω_{21} exceeds a certain value, the dark, nonabsorbing state $|+3/2\rangle_G$ is depopulated by the spin rotation in the effective field $\tilde{\mathbf{H}} = (H_x, 0, \tilde{H}_z)$. At the second crossing point, even the magnetic field of the Earth may lead to a level repulsion frequency ω_{21} of ~ 3 MHz, which is far beyond the limit found in [33] (where nuclear-spin states anticrossings are considered and this effect is negligible). Also, hyperfine interaction of the chromium electron spin with the nuclear spins of the neighboring ^{27}Al ions creates static scattering of the local field \tilde{H}_z experienced by each Cr^{3+} site [9]. These local fields are static because the hyperfine interaction creates a frozen core or diffusion barrier with suppressed spin flips of nearest nuclear-spin neighbors [36,37]. According to [9], the local field scattering is $\delta \tilde{H}_z = 6.5$ G, which results in the inhomogeneous broadening of the electron-spin resonance line with HWHM of 18 MHz. Appreciable scattering in the \tilde{H}_z value spreads the anticrossings, and their excitation by the monochromatic laser beam becomes ineffective.

These two hindrances for the trapping of Cr^{3+} in the dark state can be avoided by bichromatic excitation if the frequency difference $\Omega = \omega_1 - \omega_2$ of the two driving fields ω_1 and ω_2 well exceeds 18 MHz. Using a standard acousto-optic modulator allows getting two frequencies from the laser beam separated by 600 MHz. Because the induced magnetization will rotate with the frequency difference Ω of the driving fields, the choice of 600 MHz is good from the point of view of the spin rotation detection by the pickup coil, since for this case we are still in the RF band. Figure 2 presents the excitation of the chromium spin by a left-hand polarized bichromatic field. To match the frequency difference Ω of the driving fields to the level repulsion frequency ω_{21} at exact crossing, the tilting angle θ of the external magnetic field with respect to the optic axis has to be $\sim 1.72^\circ$, which corresponds to the transverse component of the magnetic field $H_x = 124.5$ G, while H_z is set by the condition of the level crossing. Assuming that the nuclear spin states of ^{27}Al do not cross at the electron-spin states crossing of Cr^{3+} , we can neglect the contribution of the hyperfine field to the H_x component. This is reasonable, since the transverse components of the nuclear spins oscillate with a frequency defined mostly by the H_z part of the magnetic field and their effect is averaged to zero. The longitudinal component of the hyperfine field is scattered over the range defined by the value $\delta \tilde{H}_z = 6.5$ G. The repulsion energy is described by Eq. (6), where the term $\bar{V}/h = 600$ MHz is much larger than the scattering of the diagonal contribution $\delta|\bar{\Delta}/h| = 18$ MHz. Therefore, the resultant scattering of the repulsion frequency

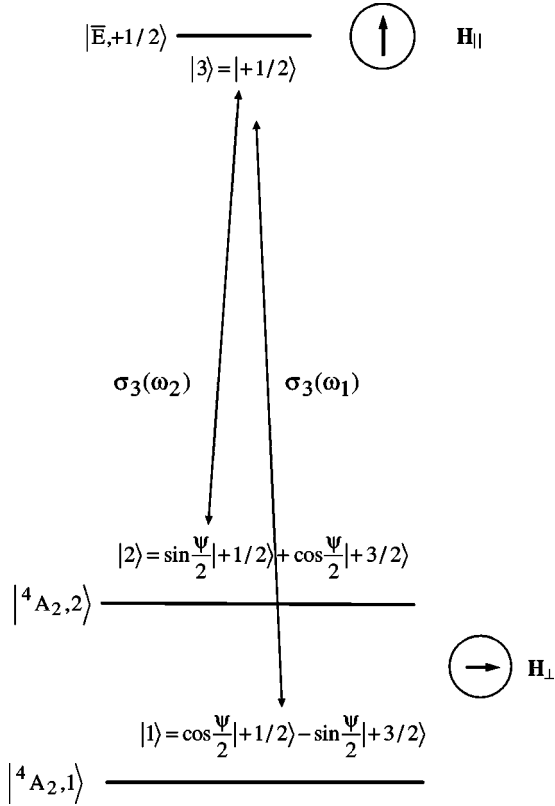


FIG. 2. Bichromatic excitation of the anticrossed states $|^4A_{2,1}\rangle$ and $|^4A_{2,2}\rangle$. \mathbf{H}_{\parallel} is an effective field seen by the spin 1/2 in the excited state \bar{E} along the z axis. \mathbf{H}_{\perp} is the transverse component of the external magnetic field that plays a dominant role at the level crossing.

is reduced to the value $\delta\omega_{21}/2\pi = 0.27$ MHz. If the Rabi frequency exceeds this value, then we can neglect the inhomogeneous broadening of the level repulsion frequency.

III. MASTER EQUATIONS FOR THE SPIN POLARIZATION

The excitation of the three-level system, shown in Fig. 2, by two driving fields ω_1 and ω_2 , is described by the master equations (see, for example, [38–40])

$$\dot{\rho}_{11} = i(B_{13}\sigma_{31} - B_{31}\sigma_{13}) + R_{11}, \quad (10)$$

$$\dot{\rho}_{22} = i(B_{23}\sigma_{32} - B_{32}\sigma_{23}) + R_{22}, \quad (11)$$

$$\dot{\rho}_{33} = -i(B_{13}\sigma_{31} - B_{31}\sigma_{13}) - i(B_{23}\sigma_{32} - B_{32}\sigma_{23}) + R_{33}, \quad (12)$$

$$\dot{\sigma}_{13} = (i\Delta_1 - \Gamma)\sigma_{13} + iB_{13}(\rho_{33} - \rho_{11}) - iB_{23}\sigma_{12}, \quad (13)$$

$$\dot{\sigma}_{23} = (i\Delta_2 - \Gamma)\sigma_{23} + iB_{23}(\rho_{33} - \rho_{22}) - iB_{13}\sigma_{21}, \quad (14)$$

$$\dot{\sigma}_{12} = [i(\omega_{21} - \Omega) - \Gamma_M]\sigma_{12} + i(B_{13}\sigma_{32} - B_{32}\sigma_{13}), \quad (15)$$

where ρ_{nn} are the density matrix elements; 1 and 2 are the ground-state sublevels, the level 3 is the excited state;

$\sigma_{12} = \rho_{12}\exp(-i\Omega t)$; $\sigma_{13} = \rho_{13}\exp(-i\omega_1 t + i\mathbf{k}\cdot\mathbf{z})$; $\sigma_{23} = \rho_{23}\exp(-i\omega_2 t + i\mathbf{k}\cdot\mathbf{z})$; \mathbf{k} is the wave vector of the laser beam, parallel to the c axis of the crystal; $\Delta_1 = \omega_{31} - \omega_1$ and $\Delta_2 = \omega_{32} - \omega_2$ are the detuning parameters of the field components ω_1 and ω_2 , respectively; R_{nn} are relaxation terms ($n=1,2,3$) describing the spontaneous decay of the excited state, spin-lattice relaxation of the ground sublevels, etc. The explicit expression for the R_{nn} will be given in the section where the steady-state solution is considered. The values Γ and Γ_M are the dephasing rates of the optical transition and ground-state spin coherence, respectively; $B_{13} = ad_{13}E/\hbar$; $B_{23} = bd_{23}E/\hbar$; $d_{13} = d_{23} = d$ is the matrix element (supposed real) of the dipole transition from the states 1,2 to the state 3 (the optical transition); E is the amplitude of the laser pump. The coefficients $a = \cos\psi/2$ and $b = \sin\psi/2$ come from the wave-function coefficients [see Eqs. (7) and (8)] for the transitions allowed because of level mixing. We suppose that both frequency components of the pump have the same amplitude and their frequency difference $\Omega = \omega_1 - \omega_2$ coincides with the level repulsion frequency ω_{21} .

Similar equations were applied to treat the Raman heterodyne detection of nuclear magnetic resonance in solids [40,41].

IV. DYNAMICAL EVOLUTION OF THE SYSTEM

First we consider the dynamical evolution of the system on a time scale much shorter than any relaxation time. In this case, all decay terms can be omitted. Brewer and Hahn [39] have shown that the coherent two-photon processes in the three-level system could be described by Blochlike equations (Bloch-vector model) in some pseudospace by introducing new variables. We define also new variables

$$n_{12} = \rho_{11} + \rho_{22}, \quad (16)$$

$$u_{12} = \sigma_{12} + \sigma_{21}, \quad (17)$$

$$V = -i(\sigma_{13} - \sigma_{31}) - i(\sigma_{23} - \sigma_{32}), \quad (18)$$

which are, however, slightly different from those in [39]. We assume that the states $|1\rangle$ and $|2\rangle$ are equally populated and the initial condition before switching on the laser beam is $n_{12}(0) = 1$, $\rho_{33}(0) = u_{12}(0) = V(0) = 0$. To simplify the calculation, we take the case $B_{13} = B_{23} = B$ corresponding to $\psi = \pi/2$. Then the Eqs. (10)–(15) can be reduced to

$$\dot{n}_{12} = \dot{u}_{12} = -\dot{\rho}_{33} = BV, \quad (19)$$

$$\dot{V} = 2B(2\rho_{33} - n_{12} - u_{12}), \quad (20)$$

where we neglect all relaxation terms and imply the resonant condition $\Delta_1 = \Delta_2 = 0$. The solution of Eqs. (19) and (20) is

$$n_{12}(t) = 1 - \frac{1}{4}(1 - \cos\chi t), \quad (21)$$

$$\rho_{33}(t) = -u_{12}(t) = \frac{1}{4}(1 - \cos\chi t), \quad (22)$$

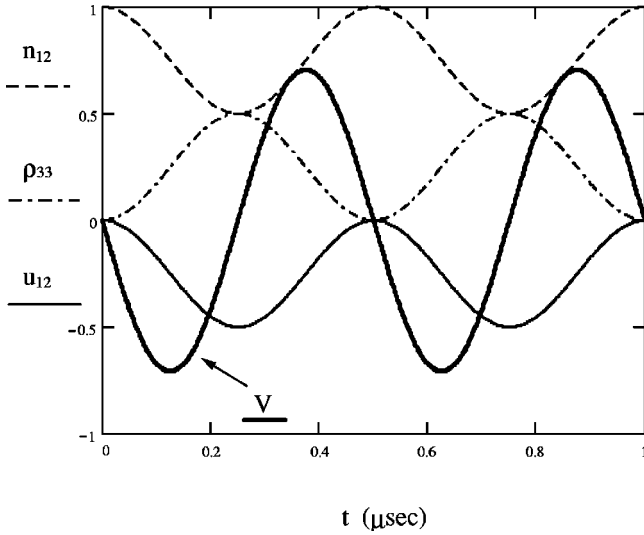


FIG. 3. The time dependences of the excited state population $\rho_{33}(t)$ (dashed-dotted line), of the sum of the population of the levels 1 and 2, $n_{12}(t) = \rho_{11}(t) + \rho_{22}(t)$ (dashed line), of the spin coherence $u_{12}(t) = \sigma_{12}(t) + \sigma_{21}(t)$ (thin solid line), and of the sum of the optical coherences $V(t) = -i(\sigma_{13} - \sigma_{31}) - i(\sigma_{23} - \sigma_{32})$ (bold solid line). They are calculated for the initial condition $\rho_{33}(0) = u_{12}(0) = V(0) = 0$ and $n_{12}(0) = 1$, if the contribution of the relaxation terms is negligible and both components of the driving field are in resonance, i.e., $\Delta_1 = \Delta_2 = 0$. The Rabi frequency is taken as $\chi/2\pi = 2$ MHz. Time scale is in microseconds.

$$V(t) = -\frac{\sqrt{2}}{2} \sin \chi t, \quad (23)$$

where $\chi = 2\sqrt{2}B = 2dE/\hbar$ is a modified Rabi frequency for a two-quantum excitation. The time dependence of the functions (21)–(23) is presented in Fig. 3. The coherence of the spin states u_{12} appears and oscillates with the Rabi frequency χ . The value of this coherence is always negative, oscillating between 0 and $-1/2$. The population of the excited state ρ_{33} rises and oscillates between 0 and $1/2$. It is worth mentioning that, in contrast to the two-level system, it is impossible to transfer all the population of the ground state to the excited state by pulse excitation. This means that conventional π -pulse excitation is impossible for this kind of three-level system. When the spin coherence u_{12} reaches the extremum $-1/2$, the optical coherence V becomes zero, although its derivative takes a maximum value. At this point V changes sign, so the process of the energy absorption by the three-level system is changed into emission. The strong influence of the spin coherence on the absorption and emission processes of the optical quanta is caused by the interference of the transition paths. This interference is positive and results in absorption if the coherence is absent. During the excitation, the spin coherence rises and makes the interference negative reducing the absorption. So, we get a new resistance channel for the excitation of the multilevel system.

The rise of the coherence between the states $|1\rangle$ and $|2\rangle$, being equally populated before the pulse, appears due to the transfer of the large population difference between the ground-state spin sublevels and the optically excited state. It

can be shown easily that, if all three states are equally populated, $\rho_{11}(0) = \rho_{22}(0) = \rho_{33}(0) = 1/3$, the spin coherence does not appear since

$$u_{12}(t) = \frac{1}{4} [2\rho_{33}(0) - n_{12}(0)](1 - \cos \chi t) \quad (24)$$

and the expression in square brackets equals zero at the imposed condition.

V. NONRESONANT EXCITATION

At liquid-helium temperature, the R_1 -line of ruby is inhomogeneously broadened with HWHM ~ 3 GHz. Therefore the laser beam excites the resonant as well as nonresonant Cr^{3+} ions. To estimate the net excited magnetization, we have to calculate the spin coherence for all (resonant and nonresonant) spectral packets.

The description of the dynamics of the nonresonant chromium impurities ($\Delta_1 \neq 0$ and $\Delta_2 \neq 0$) requires a larger number of elements of the three-level system density matrix. Aside from combinations of the density matrix elements, introduced in Eqs. (16)–(18), other components become non-zero. To describe them we define an extended set of the variables:

$$u_{13} = \sigma_{13} + \sigma_{31}, \quad (25)$$

$$u_{23} = \sigma_{23} + \sigma_{32}, \quad (26)$$

$$v_{13} = -i(\sigma_{13} - \sigma_{31}), \quad (27)$$

$$v_{23} = -i(\sigma_{23} - \sigma_{32}), \quad (28)$$

$$v_{12} = -i(\sigma_{12} - \sigma_{21}). \quad (29)$$

The following equations now describe the three-level system, still without any relaxation process:

$$\dot{\rho}_{11} = Bv_{13}, \quad (30)$$

$$\dot{\rho}_{22} = Bv_{23}, \quad (31)$$

$$\dot{\rho}_{33} = -B(v_{13} + v_{23}), \quad (32)$$

$$\dot{u}_{12} = B(v_{13} + v_{23}) - (\Delta_1 - \Delta_2)v_{12}, \quad (33)$$

$$\dot{v}_{12} = -B(u_{13} - u_{23}) + (\Delta_1 - \Delta_2)u_{12}, \quad (34)$$

$$\dot{u}_{13} = -\Delta_1 v_{13} + Bv_{12}, \quad (35)$$

$$\dot{u}_{23} = -\Delta_2 v_{23} - Bv_{12}, \quad (36)$$

$$\dot{v}_{13} = \Delta_1 u_{13} + B(2\rho_{33} - 2\rho_{11} - u_{12}), \quad (37)$$

$$\dot{v}_{23} = \Delta_2 u_{23} + B(2\rho_{33} - 2\rho_{22} - u_{12}). \quad (38)$$

We do not consider a solution of the total set of Eqs. (30)–(38), because we are only interested in the evolution of the spin coherences u_{12} and v_{12} . To avoid tedious calculations,

let us consider, for example, Eq. (33). If the evolution of the v_{13} and v_{23} components is known and $\Delta_1 = \Delta_2$ ($\Omega = \omega_{21}$), the time dependence of the u_{12} component can be calculated by taking the time integral.

As it is shown in [39], the evolution of the three-level system, driven by a bichromatic field, can be described within the Bloch-vector model, if $\Delta_1 = \Delta_2 = \Delta$ and the variables U , V and W are introduced, where V is defined in Eq. (18) and the others are

$$U = u_{13} + u_{23}, \quad (39)$$

$$W = \frac{1}{\sqrt{2}}(2\rho_{33} - n_{12} - u_{12}). \quad (40)$$

They form the Bloch-vector components, satisfying the Bloch equations

$$\dot{U} = -\Delta V, \quad (41)$$

$$\dot{V} = \Delta U + \chi W, \quad (42)$$

$$\dot{W} = -\chi V. \quad (43)$$

The solution of the Bloch equations is well known (see, for example, Ref. [1]). The components in which we are interested have the following time dependence:

$$v_{13}(t) + v_{23}(t) = V(t) = -\frac{\chi \sin(\sqrt{\Delta^2 + \chi^2}t)}{\sqrt{2(\Delta^2 + \chi^2)}}, \quad (44)$$

where the initial condition $W(0) = -1/\sqrt{2}$, $V(0) = U(0) = 0$ is taken into account. Substitution of the value $V(t)$ [Eq. (44)] into Eq. (33) and evaluation of the time integral gives the result

$$u_{12}(t) = \int_0^t BV(\tau)d\tau = -\frac{\chi^2}{4(\chi^2 + \Delta^2)}[1 - \cos(\sqrt{\Delta^2 + \chi^2}t)]. \quad (45)$$

According to this solution, the absolute value of the coherence u_{12} decreases with the increase of the detuning Δ .

It can be shown by straightforward algebra that, if $\rho_{11}(0) = \rho_{22}(0)$ and $\Delta_1 = \Delta_2 = \Delta$, the v_{12} component is still zero during the excitation as well as the population difference of the levels 1 and 2 and the difference of the other components defined in Eqs. (25)–(28), i.e.,

$$v_{12}(t) = 0, \quad (46)$$

$$\rho_{11}(t) - \rho_{22}(t) = 0, \quad (47)$$

$$u_{13}(t) - u_{23}(t) = 0, \quad (48)$$

$$v_{13}(t) - v_{23}(t) = 0. \quad (49)$$

At the previously mentioned conditions, these values satisfy the independent (closed) set of differential equations that do not include other variables. Since the values, Eqs. (46)–(49),

are not related to the n_{12} component, the only variable that is not zero at $t=0$, they do not rise during the laser excitation. This is the reason why the v_{12} component remains zero.

VI. CALCULATION OF THE SPIN MAGNETIZATION INDUCED BY LASER PUMPING

The density matrix elements $n_{12} = \rho_{11} + \rho_{22}$, $\sigma_{12} = \rho_{12} \exp(-i\Omega t)$, related to the ground states $|1\rangle$ and $|2\rangle$ [see Eqs. (7) and (8)] where the ground-state Hamiltonian Eq. (9), is diagonal. One can diagonalize this Hamiltonian by the unitary transformation

$$\hat{U} = \exp(i\psi S_y) \quad (50)$$

corresponding to the rotation of the reference frame around the y axis by the angle

$$\psi = \tan^{-1} \left(\frac{\sqrt{3}g_x \beta H_x}{g_z \beta H_z - 2D} \right). \quad (51)$$

In the case of $g_z \beta H_z = 2D$, we have $\psi = \pi/2$. This means a rotation over $\pi/2$ and the new components of the fictitious spin $\tilde{S} = 1/2$ are related to the former ones as follows:

$$\tilde{S}_{z'} = \tilde{S}_x, \quad (52)$$

$$\tilde{S}_{x'} = -\tilde{S}_z, \quad (53)$$

$$\tilde{S}_{y'} = \tilde{S}_y, \quad (54)$$

where x' , y' , and z' are the axes of the new reference frame. After the transformation, the Hamiltonian Eq. (9), takes the form

$$\tilde{H}_{eff} = \hat{U} \mathcal{H}_{eff} \hat{U}^\dagger = \tilde{g}_x \beta H_{z'} \tilde{S}_{z'}, \quad (55)$$

where $H_{z'} = H_x$ is a magnetic field defined in the new reference frame (x', y', z') . The expectation values of the operators $\tilde{S}_{x'}$, $\tilde{S}_{y'}$ and $\tilde{S}_{z'}$ can be calculated directly by the expression

$$\langle \tilde{S}_{x', y', z'} \rangle = \text{Tr}(\tilde{S}_{x', y', z'} \hat{\rho}), \quad (56)$$

where $\hat{\rho}$ is defined in the diagonal basis of the Hamiltonian (55). If $\Delta_1 = \Delta_2 = 0$ and the initial condition is $\rho_{11}(0) = \rho_{22}(0) = 1/2$ and $u_{12}(0) = v_{12}(t) = 0$, one can find that

$$\langle \tilde{S}_{x'} \rangle = \frac{1}{2} u_{12}(t) \cos \Omega t, \quad (57)$$

$$\langle \tilde{S}_{y'} \rangle = -\frac{1}{2} u_{12}(t) \sin \Omega t, \quad (58)$$

$$\langle \tilde{S}_{z'} \rangle = 0, \quad (59)$$

where $\Omega = \omega_1 - \omega_2$ is the frequency difference of the two optical driving fields ω_1 and ω_2 . Since the spin operators of the fictitious spin in the reference frames (x, y, z) and (x', y', z') are related by Eqs. (52)–(54), the corresponding

expectation values are related in a similar way and the magnetization $\mathbf{m}(t)$, produced by an individual impurity, is

$$m_x(t) = -\tilde{g}_x \beta \langle \tilde{S}_x(t) \rangle = -\tilde{g}_x \beta \langle \tilde{S}_{x'}(t) \rangle, \quad (60)$$

$$m_y(t) = -\tilde{g}_y \beta \langle \tilde{S}_y(t) \rangle = -\tilde{g}_y \beta \langle \tilde{S}_{y'}(t) \rangle, \quad (61)$$

$$m_z(t) = -g_z \beta \langle \tilde{S}_z(t) \rangle = g_z \beta \langle \tilde{S}_{z'}(t) \rangle. \quad (62)$$

We study the process of magnetization creation in ruby at liquid-helium temperature. Because the R_1 line in ruby is inhomogeneously broadened at this temperature and its HWHM is about 3 GHz, the laser beam excites only a small fraction of the chromium impurities. Bichromatic excitation induces the magnetization of the mixed states oscillating at the frequency difference Ω of the spectral components ω_1 and ω_2 . According to Eq. (45), the amplitude of the magnetization oscillates also at the Rabi frequency $\sqrt{\Delta^2 + \chi^2}$. These frequencies are different for the different spectral packets. Therefore, the pickup coil will see an average signal. We assume that $dE/h = 1$ MHz, so $\chi/2\pi = 2$ MHz, which is a reasonable value [11]. The latter is still three orders of magnitude smaller than the inhomogeneous HWHM. As a result, we have a large scattering of the modulation frequency $\sqrt{\Delta^2 + \chi^2}$.

As was shown above, the coherence u_{12} is related to the average values $\langle \tilde{S}_{x'} \rangle$, $\langle \tilde{S}_{y'} \rangle$, and $\langle \tilde{S}_{z'} \rangle$ of the fictitious spin \tilde{S} ($\tilde{S} = 1/2$). At exact crossing ($\psi = \pi/2$), we have only oscillation of the $\langle \tilde{S}_{x'} \rangle$ and $\langle \tilde{S}_{y'} \rangle$ components. The contribution of an individual impurity to the signal, detected by the pickup coil, differs in the modulation frequency $\sqrt{\Delta^2 + \chi^2}$ of the amplitude and has the same carrier frequency Ω . Below, we show that averaging over the inhomogeneous broadening results in the decay of the modulation, although does not make the average amplitude zero. This is different from a behavior of polarization induced by the resonant field in the ensemble of two-level particles with strong inhomogeneous broadening. The transient oscillation and the net amplitude of polarization averaged over the scattering of the resonant frequencies decay rapidly to zero after the switch on the field, which results from the averaging of the dynamical solution of the Bloch equations for the polarization [1].

In our case, the average value of the spin coherence is

$$\langle u_{12}(t) \rangle_{\Delta} = \int_{-\infty}^{\infty} f(\Delta) u_{12}(\Delta, t) d\Delta, \quad (63)$$

where $f(\Delta)$ is a distribution function of the optical transition frequency caused by the crystal imperfections (inhomogeneous broadening) and $u_{12}(\Delta, t)$ is defined in Eq. (45). Because HWHM of $f(\Delta)$ is much larger than χ , the integral is simplified as

$$\langle u_{12}(t) \rangle_{\Delta} = -f(0) \frac{\chi^2}{4} \int_{-\infty}^{\infty} \frac{1 - \cos(\sqrt{\Delta^2 + \chi^2} t)}{\Delta^2 + \chi^2} d\Delta, \quad (64)$$

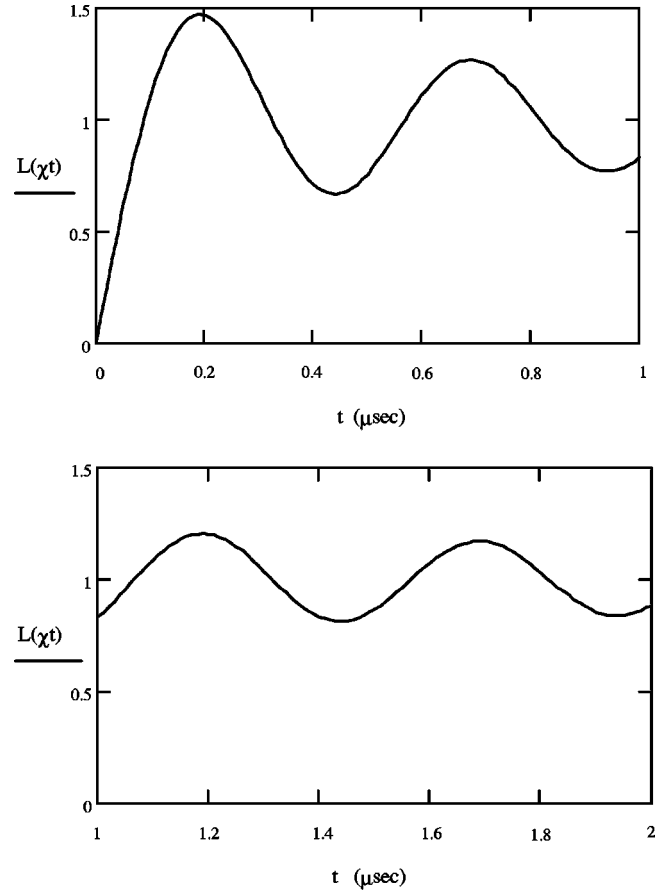


FIG. 4. Time dependence of the $L(\chi t)$ function, Eq. (66). This function shows the evolution of the spin coherence, Eq. (65), averaged over inhomogeneous broadening of the R_1 absorption line. The function $L(\chi t)$ also represents the time evolution of the amplitude of the net spin magnetization induced by the laser beam in the sample. The Rabi frequency is taken as $\chi/2\pi = 2$ MHz. Time scale is in microseconds.

where it is supposed that we excite the center of the inhomogeneous line. This integral can be calculated exactly (see, for example, Refs. [42,43]):

$$\langle u_{12}(t) \rangle_{\Delta} = -f(0) \frac{\pi}{4} \chi L(\chi t), \quad (65)$$

where

$$L(\chi t) = \int_0^{\chi t} J_0(x) dx, \quad (66)$$

and $J_0(x)$ is a zeroth-order Bessel function. $L(\chi t)$ is presented in Fig. 4. One can find the analysis of the function $L(\chi t)$ in Refs. [42–44]. This function rises from 0 to 1 almost linearly for $0 \leq \chi t \leq 1$. The value 1 is reached at $\chi t \approx 1.108$. Then the function $L(\chi t)$ oscillates slightly near the value 1 with a damped amplitude. For $\chi t \rightarrow \infty$ we have $L(\chi t) \rightarrow 1$. At the same time, the average optical polarization $\langle v_{13}(t) + v_{23}(t) \rangle_{\Delta} = \langle V(t) \rangle_{\Delta}$ [see Eq. (44)] decays as

$$\langle V(t) \rangle_{\Delta} = \int_{-\infty}^{\infty} f(\Delta) V(\Delta, t) d\Delta = -f(0) \frac{\pi}{\sqrt{2}} \chi J_0(\chi t), \quad (67)$$

since $J_0(\chi t) \rightarrow 0$ if $\chi t \rightarrow \infty$. The averaged spin coherence $\langle u_{12}(t) \rangle_{\Delta}$ does not vanish with time because it is a time integral of the optical coherence [see Eq. (45)].

The pickup coil will detect the signal with the following components:

$$M_y(t) = -\frac{\pi}{8} g_x \beta N \mathcal{V} f(0) \chi L(\chi t) \sin \Omega t, \quad (68)$$

$$M_z(t) = -\frac{\pi}{8} g_z \beta N \mathcal{V} f(0) \chi L(\chi t) \cos \Omega t, \quad (69)$$

where the average over the inhomogeneous broadening is taken into account. N is the concentration of the chromium particles in the sample and \mathcal{V} is the volume of the laser-particles interaction. These spin components do not decay to zero as $L(\chi t)$ tends to 1 when $\chi t \rightarrow \infty$.

VII. STEADY-STATE SOLUTION OF THE MASTER EQUATIONS AND ANALYSIS OF THE DARK-STATE POPULATION

In the previous section, the dynamical evolution of the spin magnetization was calculated. The stationary value that it tends is determined by relaxation processes. One of them is the spontaneous emission from the excited state $+1/2(\bar{E})$. It can terminate in the ground states $|1\rangle$ and $|2\rangle$ (σ^+ and σ^- transitions), as well as in the state $-1/2(^4A_2)$ by emitting a linearly polarized photon. Also, spin-lattice interaction induces relaxation transitions between ground-state spin sublevels. When all these processes are taken into account, the number of the independent variables necessary to describe the system will increase. Therefore, if the spontaneous emission and spin-lattice relaxation involve other levels, the dimension of our system increases and it cannot be described within the three-level approximation. To simplify the problem, we lump all other ground-state sublevels by denoting them as level $|4\rangle$ (see Fig. 5). Of course, this is an approximation. However, the result will not change qualitatively compared to the complete consideration. The advantage of this approximation is the possibility of deducing a clear condition for the capture of the system in the dark state.

The four-level system, composed of the three-level one (Fig. 2) plus the level $|4\rangle$ (Fig. 5), which belongs to the ground-state manifold, is described by the master equations (10)–(15) and equation

$$\dot{\rho}_{44} = R_{44}. \quad (70)$$

For this model the relaxation terms R_{nn} are

$$R_{11} = -2w\rho_{11} + w(\rho_{22} + \rho_{44}) + \mathcal{W}\rho_{33}, \quad (71)$$

$$R_{22} = -2w\rho_{22} + w(\rho_{11} + \rho_{44}) + \mathcal{W}\rho_{33}, \quad (72)$$

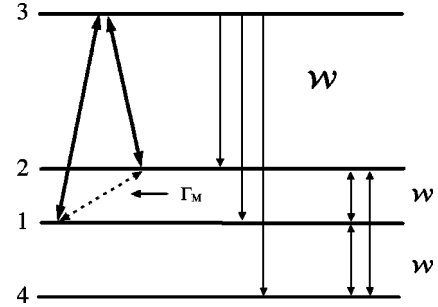


FIG. 5. Energy diagram of the four-level system chosen to describe cw excitation of ruby by a bichromatic field. \mathcal{W} and w are the spontaneous decay rate of the excited state 3 and the spin-lattice relaxation rate of the ground-state spin sublevels, respectively. Thin arrows show the corresponding transitions induced by these processes. Bold arrows show the bichromatic excitation by the laser beam. The beam is split into two frequencies by the acousto-optic modulator. The dashed line shows the induced coherence between the states 1 and 2, decaying with the rate Γ_M .

$$R_{33} = -3\mathcal{W}\rho_{33}, \quad (73)$$

$$R_{44} = -2w\rho_{44} + w(\rho_{11} + \rho_{22}) + \mathcal{W}\rho_{33}, \quad (74)$$

where \mathcal{W} is the decay rate of the excited state $|3\rangle$ and w is the rate of the spin-lattice relaxation. We do not consider w process in the excited state since even though it is faster than the spontaneous emission, it does not change the process of the dark-state population. The spin-lattice relaxation in the ground state is much slower than the spontaneous emission from the excited state ($\mathcal{W} \gg w$). The latter inequality is satisfied well since the lifetime of the excited state is 3 msec, whereas the spin-lattice relaxation time in the ground state is $(T_{1})_{spin} = 95 \pm 15$ msec for dilute ruby at liquid-helium temperature [9].

For resonant impurities ($\Delta_1 = \Delta_2 = 0$) at exact crossing ($\psi = \pi/2$), the master equation is simplified as follows:

$$\dot{u}_{12} = -\Gamma_M u_{12} + BV, \quad (75)$$

$$\dot{V} = -2Bu_{12} - \Gamma V - 2Bn_{12} + 4B\rho_{33}, \quad (76)$$

$$\dot{n}_{12} = BV - wn_{12} + 2\mathcal{W}\rho_{33} + 2w\rho_{44}, \quad (77)$$

$$\dot{\rho}_{33} = -BV - 3\mathcal{W}\rho_{33}, \quad (78)$$

$$\dot{\rho}_{44} = wn_{12} + \mathcal{W}\rho_{33} - 2w\rho_{44}. \quad (79)$$

Its stationary solution is

$$\bar{n}_{12} = \frac{2}{3 + \frac{\Gamma_M}{3w}A}, \quad (80)$$

$$\bar{u}_{12} = -\frac{1}{1 + \frac{\Gamma_M}{R} + \frac{2}{3} \frac{\Gamma_M}{\mathcal{W}}} \bar{n}_{12}, \quad (81)$$

$$\bar{\rho}_{33} = \frac{\frac{\Gamma_M}{\mathcal{W}}}{3 + 3\frac{\Gamma_M}{R} + 2\frac{\Gamma_M}{\mathcal{W}}} \bar{n}_{12}, \quad (82)$$

where $R = 2B^2/\Gamma$ is a pump parameter and

$$A = \frac{1 + 2\frac{w}{\mathcal{W}}}{1 + \frac{\Gamma_M}{R} + \frac{2}{3}\frac{\Gamma_M}{\mathcal{W}}}. \quad (83)$$

If $R \gg \Gamma_M \gg \mathcal{W} \gg w$, the parameter A is small and the population of the levels 1 and 2 becomes as small as $\bar{n}_{12} \approx 4w/\mathcal{W}$. This is a result of the selective pumping of the levels 1 and 2 and the interplay of the relaxation processes. The spontaneous transition from the state $|3\rangle$ terminates in the levels $|1\rangle$, $|2\rangle$, and $|4\rangle$ and the excitation starts only from the levels $|1\rangle, |2\rangle$. Eventually all the particles will be accumulated in the level $|4\rangle$, if the spontaneous decay (\mathcal{W}) is faster than the spin-lattice relaxation of the ground-state spin sublevels (w). The latter is responsible for recovering the Boltzmann distribution in the ground-state sublevels. The coherence \bar{u}_{12} and the population of the excited state $|3\rangle$ also become small as they are bound to the states $|1\rangle$ and $|2\rangle$ by the laser excitation.

If we have a motional narrowing effect induced by the strong driving field, the decay rate of the spin coherence Γ_M becomes as slow as the spin-lattice relaxation rate w . Then at the conditions $\mathcal{W} \gg w \sim \Gamma_M$ and $R \gg \Gamma_M$, one can find the population trapping in the coherent superposition of the states $|1\rangle$ and $|2\rangle$. The A value becomes close to 1 and the states $|1\rangle, |2\rangle$ remain populated in spite of the strong pump:

$$\bar{n}_{12} \approx \frac{2}{3 + \frac{\Gamma_M}{3w}}. \quad (84)$$

According to our model of the four-level system, the motional narrowing effect will result in the relation $\Gamma_M = \frac{3}{2}w$. However, this relation is not correct if the spin-lattice relaxation inducing the transitions $\Delta\bar{m} = \pm 1$ also engages the transitions with $\Delta\bar{m} = \pm 2$.

The level 3 is not appreciably populated according to Eq. (82). This becomes possible because of the large coherence of the ground-state levels $\bar{u}_{12} \approx \bar{n}_{12}$, preventing the excitation due to destructive interference. Figure 6 shows the dependences of the values \bar{u}_{12} and \bar{n}_{12} on the ratio Γ_M/w . If this ratio is big, the states 1 and 2 are depopulated and the spin coherence becomes negligible. Population trapping in the dark state may serve as a good mark of the motional narrowing effect. Without the suppression of the ground spin dephasing, the trapping is impossible.

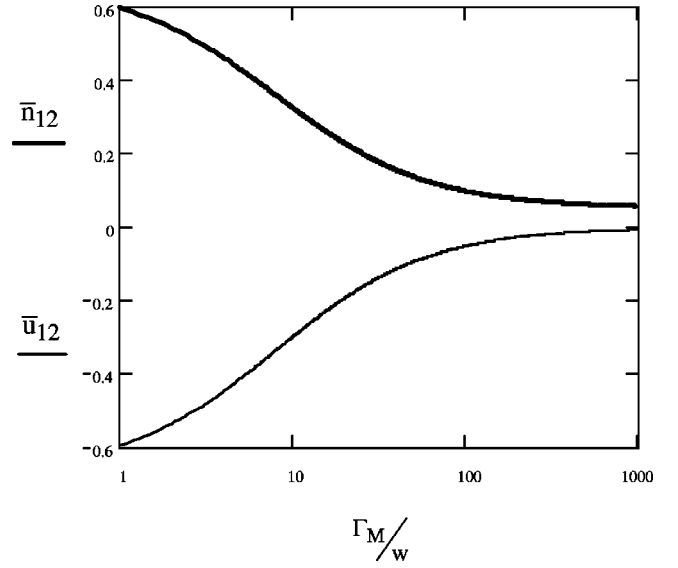


FIG. 6. The dependence of the stationary values of the spin coherence \bar{u}_{12} (thin line) and the sum of the populations of the levels 1 and 2, \bar{n}_{12} (bold line), on the ratio of the spin coherence decay rate and the spin-lattice relaxation rate, Γ_M/w . The parameters of the system are $R/2\pi = 10$ MHz, $\Delta_1 = \Delta_2 = 0$, $2w = (1/T_1)_{spin}$, and $\mathcal{W} = (1/T_1)_{opt}$, where $(T_1)_{spin} = 100$ msec and $(T_1)_{opt} = 3$ msec.

VIII. KINETICS OF THE SPIN COHERENCE

We already know the dynamic evolution of the ground-state spin coherence [see Eqs. (22), (24), and (45)] as well as the time dependence of the average magnetization, Eqs. (65) and (68) and (69), at this stage. Also, we know the stationary value of the spin coherence, Eq. (81), at cw excitation. The kinetic stage of the coherence evolution is described by the master equations (75)–(79). We do not present the analytical solution of these equations as it has a complicated form. However, we can present two plots demonstrating how the coherence of the resonant impurity reaches the stationary value. Figure 7 shows the evolution of the low-frequency coherence $u_{12}(t)$ of the resonant impurity ($\Delta_1 = \Delta_2 = 0$) if $\Gamma_M = \frac{3}{2}w$. The initial condition is $n_{12}(0) = 2/3$, $\rho_{33}(0) = 0$, and $\rho_{44}(0) = 1/3$. At the first stage, one can find the decaying Rabi oscillations. Then, at the kinetic stage of the evolution, the value $u_{12}(t)$ reaches a quasistationary, nonoscillating state with a slowly growing module. The rate of the coherence growth is proportional to the spontaneous decay rate \mathcal{W} . The ultimate value to which u_{12} tends is described by Eq. (81). For this plot, we have taken the following parameters. The Rabi frequency is $\chi/2\pi = 2$ MHz. The decay rates of the population are $\mathcal{W} = (1/T_1)_{opt}$ and $2w = (1/T_1)_{spin}$, where $(T_1)_{opt} = 3$ msec and $(T_1)_{spin} = 100$ msec, respectively. The value of the spin coherence decay Γ_M is taken such that it corresponds to the motional narrowing limit [7–9]. As for the optical coherence decay, we take the value $\Gamma = (1/T_2)_{opt}$, where $T_2 = 15$ μ sec. This value corresponds to the nonperturbed dephasing time. To be consistent, we also had to assume $(T_2)_{opt} \rightarrow (T_1)_{opt}$ at the condition of the strong excitation. However, we know that Rabi oscillations

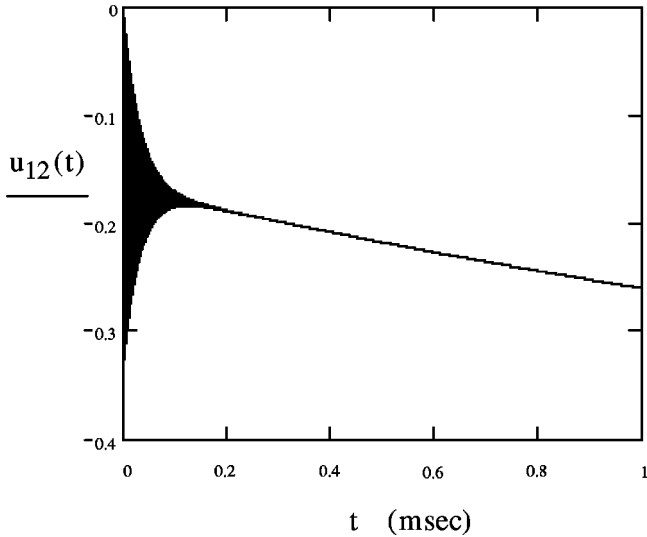


FIG. 7. The evolution of the spin coherence $u_{12}(t)$ of the resonant impurity ($\Delta_1 = \Delta_2 = 0$) for the motional narrowing limit ($\Gamma_M = \frac{3}{2}w$). The Rabi frequency is $\chi/2\pi = 2$ MHz. The initial condition is $n_{12}(0) = 2/3$, $\rho_{33}(0) = 0$, and $\rho_{44}(0) = 1/3$. Other parameters are the same as in Fig. 6. Time scale is in milliseconds.

decay fast due to the inhomogeneous broadening. The evaluation of the signal average over the inhomogeneous broadening is quite tedious and takes appreciably long computer time. Therefore, to simulate this process, we just kept the fast decay of the optical coherence that extinguishes the Rabi oscillations. This procedure allows us to show the kinetic stage of the evolution of the spin coherence. Otherwise it would be hard to distinguish the latter from the Rabi oscillations decaying with the low rate $(1/T_1)_{opt}$.

Figure 8 shows the time evolution of the spin coherence if $(T_2)_{spin}$ and $(T_2)_{opt}$ are not affected by the driving field. The coherence rises and decays on the time scale comparable with relevant dephasing rates. So, the population trapping depends strongly on the value of these decay rates.

IX. CONCLUSION

Under strong coherent excitation, the impurity, residing in the crystal, may be decoupled from the environment (neighboring spins of the host lattice and next impurities) responsible for the optical and spin coherence decay. If this process takes place, bichromatic optical excitation together with spontaneous emission are capable of creating and populating a particular superposition of the ground-state spin sublevels that does not decay. Particles trapped in this superposition state cannot absorb the optical quanta and get to the excited state. Being in the superposition of the spin states, they produce a flux variation of the magnetic field since the spin coherence oscillates with the frequency related to the energy difference of the spin states. Spin precession can be detected by a pickup coil. If the decoupling of the impurity with the environment does not take place, the bichromatic excitation produces only the short-lived spin polarization oscillating with the frequency difference of the spectral components of the driving field. Therefore, if the experiment will show the persistent oscillating magnetization, one can conclude that

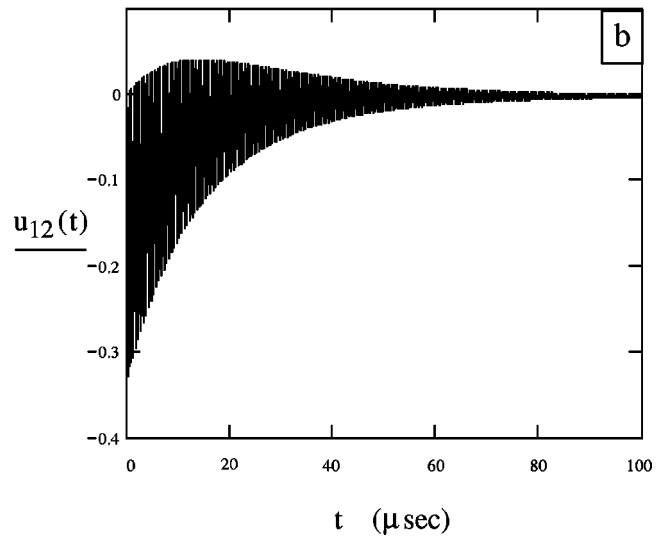
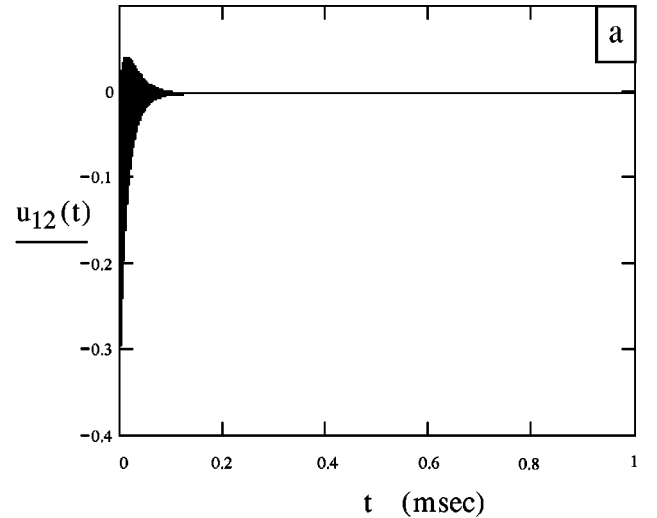


FIG. 8. The evolution of the spin coherence $u_{12}(t)$ of the resonant impurity ($\Delta_1 = \Delta_2 = 0$) for the case when motional narrowing does not occur. Decay rates of the optical coherence and spin coherence are taken as $\Gamma = (1/T_2)_{opt}$ and $\Gamma_M = (1/T_2)_{spin}$, where $(T_2)_{opt} = 15 \mu\text{sec}$ and $(T_2)_{spin} = 7.5 \mu\text{sec}$. Other parameters are the same as in Fig. 7. The plot (a) has the same time scale as in the plot of Fig. 7. The plot (b) has a ten times shorter time scale to present the details of the spin coherence evolution.

the driving field suppresses the decay of the spin coherence. If the magnetization decays with time even for a strong excitation, then it means that the decay rate of the spin coherence is faster than the spontaneous decay rate of the excited state. So, trapping in the dark state is a good test for the concept of the dephasing suppression by strong laser excitation.

ACKNOWLEDGMENTS

This work was supported by the IAP program, by the Fonds voor Wetenschappelijk Onderzoek Vlaanderen, by the Fonds National de la Recherche Scientifique Belgium, by the Belgian Federal Office for Scientific, Technical and Cultural Affairs, and by the Research Fund K.U. Leuven. Support by INTAS is also acknowledged.

- [1] L. Allen and J.H. Eberly, *Optical Resonance and Two-Level Atoms* (Wiley, New York, 1975).
- [2] E. Arimondo and G. Orriols, *Lett. Nuovo Cimento Soc. Ital. Fis.* **17**, 333 (1976).
- [3] G. Alzetta, A. Gozzini, L. Moi, and G. Orriols, *Nuovo Cimento Soc. Ital. Fis.*, B **36**, 5 (1976).
- [4] G. Alzetta, L. Moi, and G. Orriols, *Nuovo Cimento Soc. Ital. Fis.*, B **52**, 209 (1979).
- [5] G. Orriols, *Nuovo Cimento Soc. Ital. Fis.*, B **53**, 1 (1979).
- [6] E. Arimondo, in *Progress in Optics*, edited by E. Wolf (Elsevier, Amsterdam, 1966), Vol. 35, pp. 257–354.
- [7] R. Boscaino, F.M. Gelardi, and G. Messina, *Phys. Rev. A* **28**, 495 (1983).
- [8] R. Boscaino and V.M. LaBella, *Phys. Rev. A* **41**, 5171 (1990).
- [9] R. Boscaino and F.M. Gelardi, *Phys. Rev. A* **45**, 546 (1992).
- [10] R.G. DeVoe and R.G. Brewer, *Phys. Rev. Lett.* **50**, 1269 (1983).
- [11] A. Szabo and T. Muramoto, *Phys. Rev. A* **39**, 3992 (1989).
- [12] A. Szabo and R. Kaarli, *Phys. Rev. B* **44**, 12 307 (1991).
- [13] A. Abragam, *The Principles of Nuclear Magnetism* (Clarendon Press, Oxford, 1961).
- [14] A. Schenzle, M. Mitsunaga, R.G. DeVoe, and R.G. Brewer, *Phys. Rev. A* **30**, 325 (1984); *J. Opt. Soc. Am. B* **3**, 587 (1986).
- [15] E. Hanamura, *J. Phys. Soc. Jpn.* **52**, 2258 (1983); **52**, 3678 (1983).
- [16] J. Javanainen, *Opt. Commun.* **50**, 26 (1984).
- [17] P.A. Apanasevich, S.Ya. Kilin, A.P. Nizovtsev, and N.S. Onishchenko, *Opt. Commun.* **52**, 279 (1984).
- [18] M. Yamanoi and J.H. Eberly, *Phys. Rev. Lett.* **52**, 1353 (1984).
- [19] K. Wodkiewicz and J.H. Eberly, *Phys. Rev. A* **32**, 992 (1985).
- [20] P.R. Berman and R.G. Brewer, *Phys. Rev. A* **32**, 2784 (1985).
- [21] A.R. Kessel, R.N. Shakhmuratov, and L.D. Eskin, *Zh. Éksp. Teor. Fiz.* **94**, 202 (1988) [*Sov. Phys. JETP* **67**, 2071 (1988)].
- [22] R.N. Shakhmuratov, *Pis'ma Zh. Éksp. Teor. Fiz.* **51**, 454 (1990) [*JETP Lett.* **51**, 514 (1990)].
- [23] A.I. Burshtein, A.A. Zharikov, and V.S. Malinovsky, *Zh. Éksp. Teor. Fiz.* **96**, 2061 (1989) [*Sov. Phys. JETP* **69**, 1164 (1989)]; *Phys. Rev. A* **43**, 1538 (1991).
- [24] R.N. Shakhmuratov, F.M. Gelardi, and M. Cannas, *Phys. Rev. Lett.* **79**, 2963 (1997).
- [25] R.N. Shakhmuratov and A. Szabo, *Phys. Rev. A* **58**, 3099 (1998).
- [26] S. Agnello, R. Boscaino, M. Cannas, F.M. Gelardi, and R.N. Shakhmuratov, *Phys. Rev. A* **59**, 4087 (1999).
- [27] S. Sugano and Y. Tanabe, *J. Phys. Soc. Jpn.* **13**, 880 (1958).
- [28] E.O. Schulz-DuBois, *Bell Syst. Tech. J.* **38**, 271 (1959).
- [29] S. Sugano and I. Tsujikawa, *J. Phys. Soc. Jpn.* **13**, 899 (1958).
- [30] L.Q. Lambert, *Phys. Rev. B* **7**, 1834 (1973).
- [31] J.P. van der Ziel and N. Bloembergen, *Phys. Rev.* **138A**, 1287 (1965).
- [32] Y. Fukuda, Y. Takagi, K. Yamada, and T. Hashi, *J. Phys. Soc. Jpn.* **42**, 1061 (1977).
- [33] R.N. Shakhmuratov, G. Kozyreff, R. Coussement, J. Odeurs, and P. Mandel, *Opt. Commun.* **179**, 525 (2000).
- [34] A. Abragam and B. Bleaney, *Electron Paramagnetic Resonance of Transition Ions* (Clarendon Press, Oxford, 1970).
- [35] A.A. Manenkov and A.M. Prokhorov, *Zh. Éksp. Teor. Fiz.* **28**, 762 (1955) [*Sov. Phys. JETP* **1**, 611 (1955)].
- [36] N. Bloembergen, *Physica (Amsterdam)* **15**, 386 (1949).
- [37] G.R. Khutsishvili, *Comments Solid State Phys.* **5**, 23 (1972).
- [38] H.R. Schlossberg and A. Javan, *Phys. Rev.* **150**, 267 (1966).
- [39] R.G. Brewer and E.L. Hahn, *Phys. Rev. A* **11**, 1641 (1975).
- [40] N.C. Wong, E.S. Kintzer, J. Mlynek, R.G. DeVoe, and R.G. Brewer, *Phys. Rev. B* **28**, 4993 (1983).
- [41] M. Mitsunaga, E.K. Kintzer, and R.G. Brewer, *Phys. Rev. B* **31**, 6947 (1985).
- [42] A. Szabo and R.N. Shakhmuratov, *Phys. Rev. A* **55**, 1423 (1997).
- [43] R.N. Shakhmuratov, *Phys. Rev. A* **59**, 3788 (1999).
- [44] *Handbook of Mathematical Functions*, Nat. Bur. Stand. Appl. Math. Ser. No. 55, edited by M. Abramovitz and I.A. Stegun (U.S. GPO, Washington, DC, 1964).